REPORT DOCUMENTATION PAGE

Form Approved OMB NO. 0704-0188

1. REPORT DATE (DD-MM-YYYY)	2. REPORT TYPE	3. DATES COVERED (From - To)
	New Reprint	-

4. TITLE AND SUBTITLE
Separated Component-Based Restoration of Speckled SAR Images

5a. CONTRACT NUMBER
W911NF-09-1-0383

5b. GRANT NUMBER

5c. PROGRAM ELEMENT NUMBER
611103

6. AUTHORS
Vishal M. Patel, Glenn R. Easley, Rama Chellappa, Nasser M. Nasrabadi

5d. PROJECT NUMBER

5e. TASK NUMBER

5f. WORK UNIT NUMBER

7. PERFORMING ORGANIZATION NAMES AND ADDRESSES
William Marsh Rice University
Office of Sponsored Research
6100 Main St., MS-16
Houston, TX 77005 -1827

8. PERFORMING ORGANIZATION REPORT NUMBER

9. SPONSORING/MONITORING AGENCY NAME(S) AND ADDRESS(ES)
U.S. Army Research Office
P.O. Box 12211
Research Triangle Park, NC 27709-2211

10. SPONSOR/MONITOR'S ACRONYM(S)
ARO

11. SPONSOR/MONITOR'S REPORT NUMBER(S)
56177-CS-MUR.164

12. DISTRIBUTION AVAILIBILITY STATEMENT
Approved for public release; distribution is unlimited.

13. SUPPLEMENTARY NOTES
The views, opinions and/or findings contained in this report are those of the author(s) and should not contrued as an official Department of the Army position, policy or decision, unless so designated by other documentation.

14. ABSTRACT
Many coherent imaging modalities such as synthetic aperture radar suffer from a multiplicative noise, commonly referred to as speckle, which often makes the interpretation of data difficult. An effective strategy for speckle reduction is to use a dictionary that can sparsely represent the features in

15. SUBJECT TERMS
Image restoration, multiplicative noise, speckle,synthetic aperture radar.

16. SECURITY CLASSIFICATION OF:			17. LIMITATION OF ABSTRACT	15. NUMBER OF PAGES	19a. NAME OF RESPONSIBLE PERSON
a. REPORT	b. ABSTRACT	c. THIS PAGE			Richard Baraniuk
UU	UU	UU	UU		19b. TELEPHONE NUMBER 713-348-5132

Report Title

Separated Component-Based Restoration of Speckled SAR Images

ABSTRACT

Many coherent imaging modalities such as synthetic aperture radar suffer from a multiplicative noise, commonly referred to as speckle, which often makes the interpretation of data difficult. An effective strategy for speckle reduction is to use a dictionary that can sparsely represent the features in the speckled image. However, such approaches fail to capture important salient features such as texture. In this paper, we present a speckle reduction algorithm that handles this issue by formulating the restoration problem so that the structure and texture components can be separately estimated with different dictionaries. To solve this formulation, an iterative algorithm based on surrogate functionals is proposed. Experiments indicate the proposed method performs favorably compared to state-ofthe-art speckle reduction methods.

REPORT DOCUMENTATION PAGE (SF298)
(Continuation Sheet)

Continuation for Block 13

ARO Report Number 56177.164-CS-MUR
Separated Component-Based Restoration of Sp ...

Block 13: Supplementary Note

Approved for public release; distribution is unlimited.

Separated Component-Based Restoration of Speckled SAR Images

Vishal M. Patel, *Member, IEEE*, Glenn R. Easley, *Member, IEEE*, Rama Chellappa, *Fellow, IEEE*, and Nasser M. Nasrabadi, *Fellow, IEEE*

***Abstract*— Many coherent imaging modalities such as synthetic aperture radar suffer from a multiplicative noise, commonly referred to as speckle, which often makes the interpretation of data difficult. An effective strategy for speckle reduction is to use a dictionary that can sparsely represent the features in the speckled image. However, such approaches fail to capture important salient features such as texture. In this paper, we present a speckle reduction algorithm that handles this issue by formulating the restoration problem so that the structure and texture components can be separately estimated with different dictionaries. To solve this formulation, an iterative algorithm based on surrogate functionals is proposed. Experiments indicate the proposed method performs favorably compared to state-of-the-art speckle reduction methods.**

***Index Terms*— Image restoration, multiplicative noise, speckle, synthetic aperture radar.**

I. Introduction

COHERENT imaging systems such as synthetic aperture radar (SAR), holography, ultrasound, and synthetic aperture sonar suffer from a multiplicative noise known as speckle [1]. Speckle appears when objects illuminated by coherent radiation have surface features that are rough compared with the illuminating wavelength. It is caused by the constructive and destructive interference of the coherent returns scattered by many elementary reflectors within the resolution cell. Speckle can make the detection and interpretation difficult for automated as well as human observers. In some cases, it may be important to remove speckle to improve applications such as compression, target recognition, and segmentation.

Many algorithms have been developed to suppress speckle noise [2]–[7]. One of the simplest approaches for speckle noise reduction is known as multilook processing. It involves noncoherently summing the independent images formed from L independent pieces of the phase history. The averaging process reduces the noise variance by a factor of L. However, this often results in the reduction of the spatial resolution. Other types of speckle reduction methods are based on spatial local filtering performed after the formation of the SAR image. Various filters have been developed that avoid the loss in spatial resolution [2], [8]–[11]. Some of these methods are based on a window processing of the noisy image. Consequently, their performance depends significantly on the type, direction, and the size of the filter used. Furthermore, some of these filters often fail to preserve sharp features such as edges.

To overcome some of these limitations, wavelet-based methods are often utilized [12]–[17], in which noise shrinkage is applied to the detailed wavelet coefficients of the noisy image [18], [19]. Since speckle is multiplicative in nature, some of these methods often apply the logarithm transform to SAR images to convert the multiplicative noise into additive noise. After applying soft or hard thresholding to the wavelet coefficients of the logarithmically transformed image, an exponential operation is employed to convert the logarithmically transformed image back to the original multiplicative format.

It is well known that shrinkage-based denoising algorithms rely on the sparsity of the representation. A fixed transform such as a wavelet transform can represent a piecewise smooth image sparsely but it may also fail to represent an image with textures sparsely. As a result, the overall denoising performance of a fixed transform on an image containing both piecewise smooth and texture components can be inadequate.

Another popular approach for restoring speckled images involves total variation (TV) regularization [20], where the underlying reflectivity image is assumed to be piecewise smooth [21]–[23]. It has been shown that TV regularization often yields images with the staircasing effect [24]. As a result, the estimated image usually contains constant regions, and fine details such as textures are often removed. To deal with some of these effects, a hybrid method that uses coefficient thresholding and TV regularization on the logarithm of the magnitude image or the log-image domain was recently proposed [25]. In particular, hard thresholding on the curvelet coefficients of the log-image is first applied. Then a variational method that uses an ℓ_1 fidelity to the thresholded coefficients and a TV regularization in the log-image domain is applied.

Several methods have been proposed that use a combined dictionary approach to image restoration. Suppose that we are given M different dictionaries $\mathbf{D}_m$, $m = 1, \ldots, M$; then one can obtain M different estimates of $\mathbf{x}$ by applying either hard

Manuscript received November 28, 2011; revised November 22, 2012; accepted February 3, 2013. The work of V. M. Patel and R. Chellappa was supported by the Army Research Office MURI under Grant W911NF0910383.

V. M. Patel and R. Chellappa are with the Department of Electrical and Computer Engineering and the Center for Automation Research, UMIACS, University of Maryland, College Park, MD 20742 USA (e-mail: pvishalm@umiacs.umd.edu; rama@umiacs.umd.edu).

G. R. Easley is with the Norbert Wiener Center, Department of Mathematics, University of Maryland, College Park, MD 20742 USA (e-mail: geasley@math.umd.edu).

N. M. Nasrabadi is with the U.S. Army Research Laboratory, Adelphi, MD 20783 USA (e-mail: nasser.m.nasrabadi@us.army.mil).

Color versions of one or more of the figures in this paper are available online at http://ieeexplore.ieee.org.

Digital Object Identifier 10.1109/TGRS.2013.2246794

or soft threshold to the coefficients from each corresponding dictionary. Let $\hat{\mathbf{x}}_i$ be the resulting estimate from the ith dictionary. Then, a simple estimator of $\mathbf{x}$ is given by averaging M individual estimates

$$\hat{\mathbf{x}} = \frac{1}{M}\sum_{i=1}^{M}\hat{\mathbf{x}}_i.$$

This is essentially the idea behind translation-invariant wavelet denoising by cycle spinning [26], where the final estimate is obtained by averaging the estimates from the thresholded orthogonal wavelet coefficients of translated versions of the original image. This method has been applied for speckle reduction in SAR imagery [12]. This simple method suffers from some issues in practice, as it weighs equally both good and bad quality estimates. To deal with this problem, a Bayesian framework to optimally combine the individual estimators was proposed in [27]. This method weights each estimate $\hat{\mathbf{x}}_i$ at each sample according to the significance that the elements in the dictionary $\mathbf{D}_i$ have in synthesizing $\hat{\mathbf{x}}_i$ at the same sample. This method is effective, but it can be very time consuming. A similar approach was also proposed in [28].

A novel cartoon and texture image component-based restoration for SAR images was proposed in [29]. Specifically, a SAR image, considered as a function f, is to be decomposed into a sum of two components $f = u + v$, where u represents the cartoon or geometric (i.e., piecewise smooth) components of f, and v represents the oscillatory or textured components. The second component essentially accounts for noise and the texture elements. In the proposed technique, u is estimated and is considered as the restored (despeckled) image, while the textured components of v are not attempted to be recovered. This is problematic since discarding the texture components may result in the loss of important salient features in a SAR image. Fig. 1 provides an example of how an image separates into the structural and textured components indicating the importance of retaining these textural elements.

Motivated by recent advances in sparse representation-based image separation [30], we propose a similar separation-based despeckling method so that the image is decomposed into a sum of piecewise smooth and textured elements. Our formulation is based on finding sparse representations of these elements from dictionaries specifically suited to compress them, and differs significantly by not just treating the texture and noise components as complements of the cartoon-based estimated image. By taking advantage of the ability of sparse representations in our scheme to estimate, we are able to retain important salient and textured features in the final estimated image.

A. Organization of This Paper

Section II reviews the statistical models for SAR images. In Section III, we present the component separation algorithm based on surrogate functionals. In Section IV, we show some of the results on both real and simulated data. We present the concluding remarks in Section V.

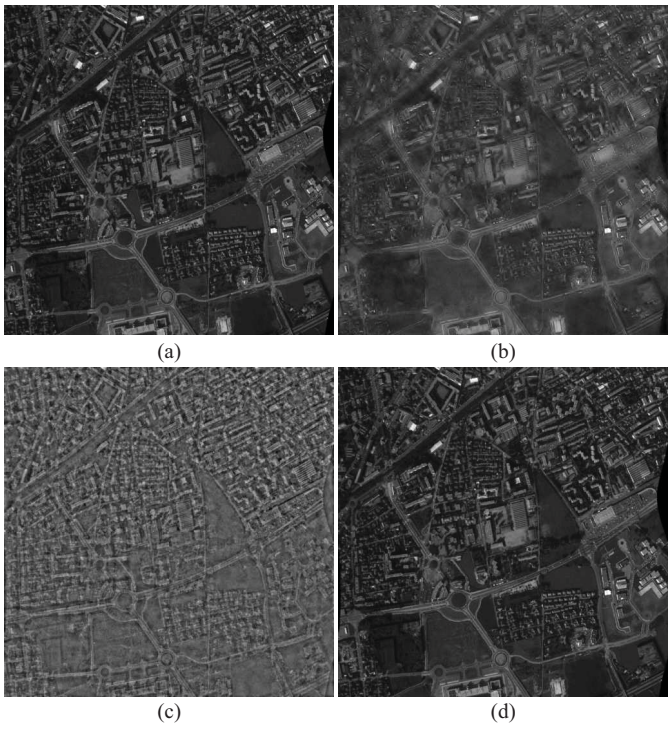

Fig. 1. Image separation. (a) Original image. (b) Structural components. (c) Textural components. (d) Structural + textural components. Note that the textural components in (c) contain some important features.

II. Statistical Models for SAR Images

Let $Y \in \mathbb{R}^{N\times N}$ be the observed image intensity, $X \in \mathbb{R}^{N\times N}$ be the noise free image, and $F \in \mathbb{R}^{N\times N}$ be the speckle noise. Assuming the SAR image represents an average of L looks, Y is related to X by the following multiplicative model [31]:

$$Y = FX \tag{1}$$

where F is the normalized fading speckle noise random variable. It follows a gamma distribution with unit mean and variance $\frac{1}{L}$ and has the following probability density function (pdf):

$$p(F) = \frac{1}{\Gamma(L)}L^L F^{L-1}e^{-LF} \tag{2}$$

where $F \geq 0$, $L \geq 1$, and $\Gamma(.)$ denotes the gamma function.

The natural logarithmic transformation converts the multiplicative noise model (1) into an additive model

$$\begin{aligned}\tilde{Y} = \ln(Y) &= \ln(F) + \ln(X)\\ &= \tilde{F} + \tilde{X}\end{aligned} \tag{3}$$

where $\tilde{F} = \ln(F)$ and $\tilde{X} = \ln(X)$. The pdf of the random variable $\tilde{F}$ is given by [31], [32]

$$p(\tilde{F}) = \frac{1}{\Gamma(L)}L^L e^{\tilde{F}L}e^{-Le^{\tilde{F}}}. \tag{4}$$

The mean of $\tilde{F}$ is given by

$$E[\tilde{F}] = \psi(0, L) - \ln(L)$$

and variance is given by

$$\mathrm{var}(\tilde{F}) = \psi(1, L)$$

where

$$\psi(k,t) = \left(\frac{d}{dt}\right)^{k+1} \ln \Gamma(t)$$

is known as the kth polygamma function.

Note that there exist many statistical models for SAR images [33], some based on mathematical approaches and others based on physical approaches. In this paper, we use the logarithmic transform to convert the multiplicative noise to an additive noise and take into account the appropriate distribution model to handle the noise.

III. Image Component Estimation

Let $\mathbf{y}, \mathbf{f}$, and $\mathbf{x}$ be lexicographically ordered vectors of size N^2 representing $\tilde{Y}$, $\tilde{F}$, and $\tilde{X}$, respectively. We assume that the SAR reflectivity field is a superposition of two different signals

$$\mathbf{x} = \mathbf{x}_p + \mathbf{x}_t \tag{5}$$

where $\mathbf{x}_p$ is the piecewise smooth component of $\mathbf{x}$ and $\mathbf{x}_t$ is the texture component of $\mathbf{x}$. So the additive model (3) can be written as

$$\begin{aligned}\mathbf{y} &= \mathbf{x} + \mathbf{f} \\ &= \mathbf{x}_p + \mathbf{x}_t + \mathbf{f}.\end{aligned} \tag{6}$$

We further assume that $\mathbf{x}_p$ is compressible in a dictionary represented in a matrix form as $\mathbf{D}_p$, and similarly, $\mathbf{x}_t$ is compressible in a dictionary represented in a matrix form as $\mathbf{D}_t$. Given $M_p, M_t \geq N^2$, the dictionary $\mathbf{D}_p \in \mathbb{R}^{N^2 \times M_p}$ and $\mathbf{D}_t \in \mathbb{R}^{N^2 \times M_t}$ are chosen such that they provide sparse representations of piecewise smooth and texture contents, respectively. That is, we assume that there are coefficient vectors $\alpha_p \in \mathbb{R}^{M_p \times 1}$ and $\alpha_t \in \mathbb{R}^{M_t \times 1}$ so that $\mathbf{x}_p = \mathbf{D}_p \alpha_p$ and $\mathbf{x}_t = \mathbf{D}_t \alpha_t$. The compressibility assumption means that, when the coefficients are ordered in magnitude, they decay rapidly. The texture dictionary $\mathbf{D}_t$ needs to contain atoms that are oscillatory in nature such as those found in the discrete cosine/sine transform and the Gabor transform. The dictionary $\mathbf{D}_p$ should be able to process images with geometric features such as edges. The matrix $\mathbf{D}_p$ could represent some type of wavelet, shearlet, curvelet, or contourlet dictionary.

One can recover the SAR reflectivity field $\mathbf{x}$ by estimating the components $\mathbf{x}_p$ and $\mathbf{x}_t$ via α_p and α_t by solving the following variational problem:

$$\begin{aligned}\hat{\alpha}_p, \hat{\alpha}_t = \arg\min_{\alpha_p, \alpha_t} \lambda\|\alpha_p\|_1 + \lambda\|\alpha_t\|_1 + \gamma\, TV(\mathbf{D}_p\alpha_p) \\ + \frac{1}{2}\|\mathbf{y} - \mathbf{D}_p\alpha_p - \mathbf{D}_t\alpha_t\|_2^2\end{aligned} \tag{7}$$

where TV is the TV (i.e., sum of the absolute variations in the image) and for an N-dimensional vector $\mathbf{x}$, $\|.\|_q$ denotes the ℓ_q-norm, $0 < q < \infty$, defined as

$$\|\mathbf{x}\|_q = \left(\sum_{i=1}^{N} |x_i|^q\right)^{1/q}. \tag{8}$$

The two components are the corresponding representations of the two parts and can be obtained by $\hat{\mathbf{x}}_p = \mathbf{D}_p\hat{\alpha}_p$ and $\hat{\mathbf{x}}_t = \mathbf{D}_t\hat{\alpha}_t$. This notion of separating a signal into different morphologies using sparse representations is often known as morphological component analysis (MCA) [30].

Instead of seeking the sparse sets of coefficients α_p and α_t directly and then inverting the representations, it is possible to directly seek the images whose transform coefficients or dictionary representations are sparse. This corresponds to solving the following optimization problem:

$$\begin{aligned}\hat{\mathbf{x}}_p, \hat{\mathbf{x}}_t = \arg\min_{\mathbf{x}_p, \mathbf{x}_t} \lambda\|\mathbf{D}_p^\dagger\mathbf{x}_p\|_1 + \lambda\|\mathbf{D}_t^\dagger\mathbf{x}_t\|_1 + \gamma\, TV(\mathbf{x}_p) \\ + \frac{1}{2}\|\mathbf{y} - \mathbf{x}_p - \mathbf{x}_t\|_2^2\end{aligned} \tag{9}$$

where $\mathbf{D}_t^\dagger$ denotes the Moore–Penrose pseudo-inverse of $\mathbf{D}_t$. Here, we have assumed that the two redundant dictionaries are of full rank and we can obtain the analysis operator from the synthesis by using the following relations:

$$\begin{aligned}\alpha_p &= \mathbf{D}_p^\dagger\mathbf{x}_p \\ \alpha_t &= \mathbf{D}_t^\dagger\mathbf{x}_t.\end{aligned}$$

One of the major advantages of using (9) is that it requires searching lower dimensional vectors rather than longer dimensional representation coefficient vectors. This increases numerical efficiency and decreases memory constraints.

A. Iterative Shrinkage Algorithm

Various methods can be used to obtain the solution of (7) [34], [35]. In this section, we derive a fast convergent iterative shrinkage algorithm by a method of using separable surrogate functionals (SSF) to solve the separation problem posed in (7) [35] – [37]. For simplicity, we assume that $\mathbf{D} = [\mathbf{D}_p, \mathbf{D}_t]$ and discard the TV component for the discussion given here. The objective function in (7) can then be rewritten as

$$f(\alpha) = \lambda\|\alpha\|_1 + \frac{1}{2}\|\mathbf{y} - \mathbf{D}\alpha\|_2^2 \tag{10}$$

where α contains both the piecewise smooth and texture parts. Let

$$d(\alpha, \alpha_0) = \frac{c}{2}\|\alpha - \alpha_0\|_2^2 - \frac{1}{2}\|\mathbf{D}\alpha - \mathbf{D}\alpha_0\|_2^2 \tag{11}$$

where α_0 is an arbitrary vector of length N^2 and the parameter c is chosen such that d is strictly convex. This constraint is satisfied by choosing

$$c > \|\mathbf{D}^T\mathbf{D}\|_2 = \lambda_{\max}(\mathbf{D}^T\mathbf{D}) \tag{12}$$

where $\lambda_{\max}(\mathbf{D}^T\mathbf{D})$ is the maximal eigenvalue of the matrix $\mathbf{D}^T\mathbf{D}$.

Adding (11) to (10) gives the following surrogate function:

$$\tilde{f}(\alpha) = \lambda\|\alpha\|_1 + \frac{1}{2}\|\mathbf{y} - \mathbf{D}\alpha\|_2^2 + \frac{c}{2}\|\alpha - \alpha_0\|_2^2 - \frac{1}{2}\|\mathbf{D}\alpha - \mathbf{D}\alpha_0\|_2^2. \tag{13}$$

This surrogate function $\tilde{f}(\alpha)$ can be re-expressed as

$$\tilde{f}(\alpha) = A + \frac{\lambda}{c}\|\alpha\|_1 + \frac{1}{2}\|\alpha - \mathbf{x}_0\|^2 \tag{14}$$

where

$$\mathbf{x}_0 = \frac{1}{c}\mathbf{D}^T(\mathbf{y} - \mathbf{D}\alpha_0) + \alpha_0 \tag{15}$$

and A is some constant. Let $(a)_+$ denote the function $\max(a, 0)$, and sign(x) be the signum function defined as

$$\text{sign}(x) = \begin{cases} -1, & \text{if } x < 0 \\ 0, & \text{for } x = 0 \\ 1, & \text{for } x > 0. \end{cases}$$

Given that

$$\mathcal{S}_\lambda(\mathbf{x}) = \text{sign}(\mathbf{x})(|\mathbf{x}| - \lambda)_+ \tag{16}$$

is the element-wise soft-thresholding operator with threshold λ, the global minimizer of the surrogate function is given by

$$\begin{aligned} \alpha_{sol} &= \mathcal{S}_{\lambda/c}(\mathbf{x}_0) \\ &= \mathcal{S}_{\lambda/c}\left(\frac{1}{c}\mathbf{D}^T(\mathbf{y} - \mathbf{D}\alpha_0) + \alpha_0\right). \end{aligned} \tag{17}$$

It was shown in [36] that the iterations

$$\alpha^{k+1} = \mathcal{S}_{\lambda/c}\left(\frac{1}{c}\mathbf{D}^T(\mathbf{y} - \mathbf{D}\alpha^k) + \alpha^k\right) \tag{18}$$

converge to the minimizer of the function f in (10), where the superscript k indicates that it is the value for the kth iteration. By breaking the above iteration into the two representation parts and considering the TV term, we get the following iterative updates that essentially solves (7):

$$\tilde{\alpha}_p^{k+1} = \mathcal{S}_{\lambda/c}\left(\frac{1}{c}\mathbf{D}_p^T(\mathbf{y} - \mathbf{D}_p\hat{\alpha}_p^k - \mathbf{D}_t\hat{\alpha}_t^k) + \hat{\alpha}_p^k\right) \tag{19}$$

$$\alpha_p^{k+1} = \mathbf{D}_p^T\mathbf{H}\mathcal{S}_{\gamma^k}\left(\mathbf{H}^T\mathbf{D}_p\tilde{\alpha}_p^{k+1}\right) \tag{20}$$

$$\alpha_t^{k+1} = \mathcal{S}_{\lambda/c}\left(\frac{1}{c}\mathbf{D}_t^T(\mathbf{y} - \mathbf{D}_p\hat{\alpha}_p^k - \mathbf{D}_t\hat{\alpha}_t^k) + \hat{\alpha}_t^k\right) \tag{21}$$

where $\mathbf{H}$ is the undecimated Haar wavelet dictionary. A detailed description of the undecimated Haar wavelet transform can be found in [38]. We have replaced the TV correction term by a redundant Haar wavelet-based shrinkage estimate, as this seems to give the best results. This adjustment is applied only to the piecewise smooth component to control the ringing artifacts near the edges caused by the oscillations of the atoms in the dictionary $\mathbf{D}_p$. The same adjustment was used in [30], and the substitution was partially motivated by observing the connection between TV and the Haar wavelet given in [39].

The iterations presented above can be extended to handle the analysis formulation in (9). This is simply done by modifying iterations (19)–(21) as follows:

$$\tilde{\mathbf{x}}_p^{k+1} = \mathbf{D}_p.\mathcal{S}_{\lambda/c}\left(\frac{1}{c}\mathbf{D}_p^T(\mathbf{y} - \hat{\mathbf{x}}_p^k - \hat{\mathbf{x}}_t^k) + \mathbf{D}_p^\dagger\hat{\mathbf{x}}_p^k\right) \tag{22}$$

$$\mathbf{x}_p^{k+1} = \mathbf{H}\mathcal{S}_{\gamma^k}\left(\mathbf{H}^T\tilde{\mathbf{x}}_p^{k+1}\right) \tag{23}$$

$$\mathbf{x}_t^{k+1} = \mathbf{D}_t.\mathcal{S}_{\lambda/c}\left(\frac{1}{c}\mathbf{D}_t^T(\mathbf{y} - \hat{\mathbf{x}}_p^k - \hat{\mathbf{x}}_t^k) + \mathbf{D}_t^\dagger\hat{\mathbf{x}}_t^k\right). \tag{24}$$

We summarize the algorithm for recovering the two separated components of a SAR image in Fig. 2. In step 3 of the algorithm in Fig. 2, $\|.\|_\infty$ denotes the ℓ_∞-norm. For an N-dimensional vector $\mathbf{x}$, it is defined as $\|\mathbf{x}\|_\infty = \max(|x_1|, \ldots, |x_N|)$.

Input: $\mathbf{y}, c$.
Initialization: Initialize $k = 1$ and set $\mathbf{x}_p^0 = \mathbf{0}$, $\mathbf{x}_t^0 = \mathbf{0}$, $\mathbf{r}^0 = \mathbf{y} - \mathbf{x}_p^0 - \mathbf{x}_t^0$, and $\lambda^0 = \frac{1}{2}\left(\|\mathbf{D}_p^T\mathbf{y}\|_\infty + \|\mathbf{D}_t^T\mathbf{y}\|_\infty\right)$.
repeat:
1. Update the estimate of $\mathbf{x}_p$ and $\mathbf{x}_t$ as

$$\begin{aligned} \tilde{\mathbf{x}}_p^k &= \mathbf{D}_p.\mathcal{S}_{\lambda^k}\left(\frac{1}{c}\mathbf{D}_p^T(\mathbf{r}^{k-1}) + \mathbf{D}_p^\dagger\hat{\mathbf{x}}_p^{k-1}\right) \\ \mathbf{x}_p^k &= \mathbf{H}\mathcal{S}_{\gamma^k}\left(\mathbf{H}^T\tilde{\mathbf{x}}_p^k\right) \\ \mathbf{x}_t^k &= \mathbf{D}_t.\mathcal{S}_{\lambda^k}\left(\frac{1}{c}\mathbf{D}_t^T(\mathbf{r}^{k-1}) + \mathbf{D}_t^\dagger\hat{\mathbf{x}}_t^{k-1}\right). \end{aligned}$$

2. Update the residual as

$$\mathbf{r}^k = \mathbf{y} - \mathbf{x}_p^k - \mathbf{x}_t^k.$$

3. Update the shrinkage parameter as

$$\lambda^k = \frac{1}{2}\left(\|\mathbf{D}_p^T\mathbf{r}^k\|_\infty + \|\mathbf{D}_t^T\mathbf{r}^k\|_\infty\right).$$

until: stopping criterion is satisfied.
Output: The two components $\hat{\mathbf{x}}_p = \mathbf{x}_p^k$ and $\hat{\mathbf{x}}_t = \mathbf{x}_t^k$.

Fig. 2. SSF iterative shrinkage algorithm to solve (9).

Once the two denoised components of $\mathbf{x}$ are estimated, we obtain the final estimate of $\mathbf{x}$ as

$$\hat{\mathbf{x}} = \exp(\hat{\mathbf{x}}_p + \hat{\mathbf{x}}_t). \tag{25}$$

Since the logarithmic transformation introduces a bias on the final estimate, we correct it along with the exponential transformation [12], [25].

IV. Experimental Results

In this section, we present the results of our proposed despeckling algorithm and compare them with the enhanced Lee filter [2] and some recent state-of-the-art methods [25], [30]. We also compare our results with a Stein–Block thresholding (SBT) method proposed in [40]. This method was shown to be nearly minimax over a large class of images in the presence of additive bounded noise. This method requires a threshold parameter, which we set to the theoretical value 4.505 as derived in [40]. Furthermore, we compare the performance of our combined dictionary-based approach to despecking with that of a fixed transform-based despecking method. In particular, we apply soft thresholding on the subband coefficients of the wavelet transform. We call the resulting method wavelet-based thresholding (WT). For the MCA method [30], we use the curvelet transform to represent the piecewise smooth component and 2D-DCT to represent the texture component.

In Fig. 3, we display the test images used for different experiments in this paper. In these experiments, we use the relative error (RE) and the equivalent number of looks (ENL)

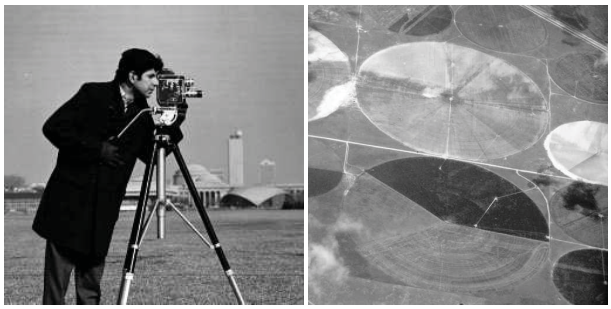

(a) (b)

(c)

Fig. 3. Images used in this paper for different experiments. (a) 256×256 *Cameraman* image. (b) 512×512 *Fields* image. (c) 512×512 *Nimes* image.

to measure the performance of the routines tested, given by

$$\text{RE} = \frac{\|\hat{\mathbf{x}} - \mathbf{x}\|_2}{\|\mathbf{x}\|_2}$$

$$\text{ENL} = \frac{\text{mean}^2}{\text{variance}}$$

where the mean and the variance are measured within a homogeneous region (see [21] and [2]). A large ENL value corresponds to better speckle reduction.

A. Dictionaries

In our experiments, we use a dictionary corresponding to the shearlet transform to represent the piecewise smooth component. Shearlets extend the traditional wavelets by allowing waveforms to be defined not only at various scales and locations but also at various orientations [41]. The shearlet transform is best suited for representing images with edges and anisotropic structures. Moreover, numerical results give evidence to the superior behavior of shearlet-based decomposition algorithms when compared to curvelet-based and contourlet-based algorithms [41], [42]. This is the reason why we choose shearlets instead of curvelets and contourlets in our approach. A brief discussion about the shearlet transform is given in the Appendix. Fig. 4 shows some atoms from a shearlet dictionary. In our implementation, we used the nonsubsampled shearlet transform with the decomposition structure [3, 3, 4, 4], which determines the number of directions in the scales from coarse to fine. As a result, the size of $\mathbf{D}_p$ is $N^2 \times 56N^2$.

The discrete cosine transform is known to closely approximate the Karhunen–Loève transform for a class of random signals known as first-order Markov processes that model several real-world images. Explicitly, the coefficients of the

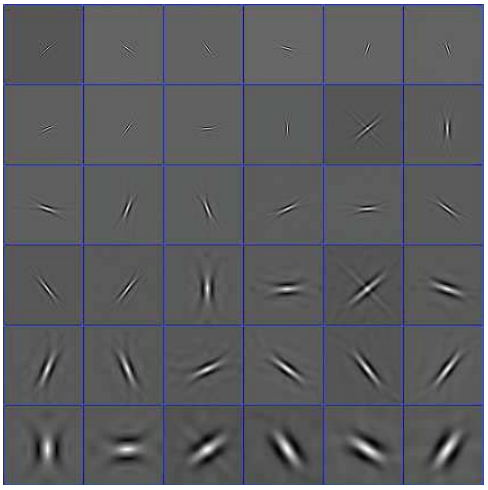

Fig. 4. Atoms from a shearlet dictionary. Each block represents the result of applying the shearlet transform for a particular scale and orientation after applying it to a centered impulse response.

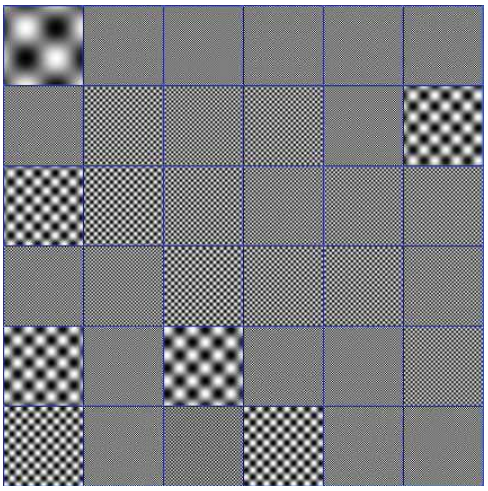

Fig. 5. Atoms from the 2D-DCT dictionary. Each block represents the result of applying the inverse 2D-DCT transform to impulse responses, which are centered at various locations.

DCT for an $N \times N$ image $x = (x_{m,n})$ are

$$X_{j,k} = \frac{2}{N} \sum_{m=0}^{N-1} \sum_{n=0}^{N-1} x_{m,n} \cos(\pi (m - 1/2)(j - 1/2)/N) \times \cos(\pi (n - 1/2)(k - 1/2)/N).$$

It is clear the oscillatory nature of the basis functions can represent repetitious elements common to texture components, which is why they are commonly used for this purpose. A few atoms from the 2D-DCT dictionary are shown in Fig. 5. The number of atoms in the dictionary $\mathbf{D}_t$ are $64 \times N^2$.

B. Parameters

From the discussion in Section III, the parameter c should be chosen such that $c > \lambda_{\max}(\mathbf{D}_p\mathbf{D}_p^T + \mathbf{D}_t\mathbf{D}_t^T)$. This can be satisfied by choosing $c > 2$. In particular, the value we chose was $c = 3$.

The Haar shrinkage value γ^k in step 1 of the algorithm is $3\sigma_{x_p}^k$, where $\sigma_{x_p}^k$ is the standard deviation of the noise estimated by using a median estimator on the finest scale of the Haar wavelet coefficients of $\tilde{\mathbf{x}}_p^k$ [19].

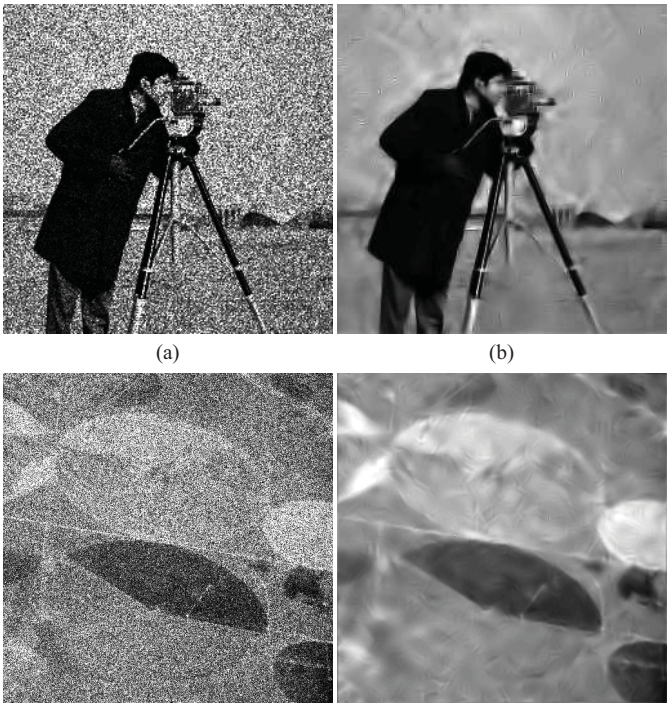

Fig. 6. (a) Noisy image, $L = 4$, $RE = 0.498$. (b) Restored image using our method, $RE = 0.118$. (c) Noisy image, $L = 4$, $RE = 0.500$. (d) Restored image using our method, $RE = 0.065$.

C. Stopping Rule

We change the threshold value of λ^k during each iteration according to

$$\lambda^k = \frac{1}{2}\left(\|\mathbf{D}_p^T\mathbf{r}^k\|_\infty + \|\mathbf{D}_t^T\mathbf{r}^k\|_\infty\right) \tag{26}$$

and stop the iterations when $\lambda^k \leq T\sigma$, where $T \approx 2.1$ [43]. This way, we stop the iterations when the residual is at the noise level and the noise is rejected in each component. Note that this step of the algorithm assumes the noise variance to be known. This is not a problem since the noise variance can easily be estimated by using a median estimator on the finest scale of the wavelet coefficients of $\mathbf{y}$ [19].

D. Results on Simulated Data

In Table I, we report the results of experiments on the simulated data with a various number of looks. We did not have access to the codes of [21], [25], and [22]. Hence, we report the RE values reported in the corresponding papers. Figs. 6 and 7 show the noisy and restored images for some of the experiments with the simulated data. It can be seen from these figures and the results in Table I that our method performs favorably over some of the competitive methods for speckle reduction. In particular, this is the case when the number of looks is greater than 3. Furthermore, these results clearly indicate that an improvement is achieved when a combined dictionary approach is used to restore a SAR image, as can be seen by comparing the results of our method with that of SBT, MCA, and WT in Table I.

Using the *Cameraman* image, in Figs. 8 and 9, we show the evolution of the objective function and RE, respectively, as we vary the number of looks. Note that in Fig. 9 the RE decreases significantly after five iterations and saturates around the 10th iteration, showing that the proposed method is efficient and requires less number of iterations compared to [21].

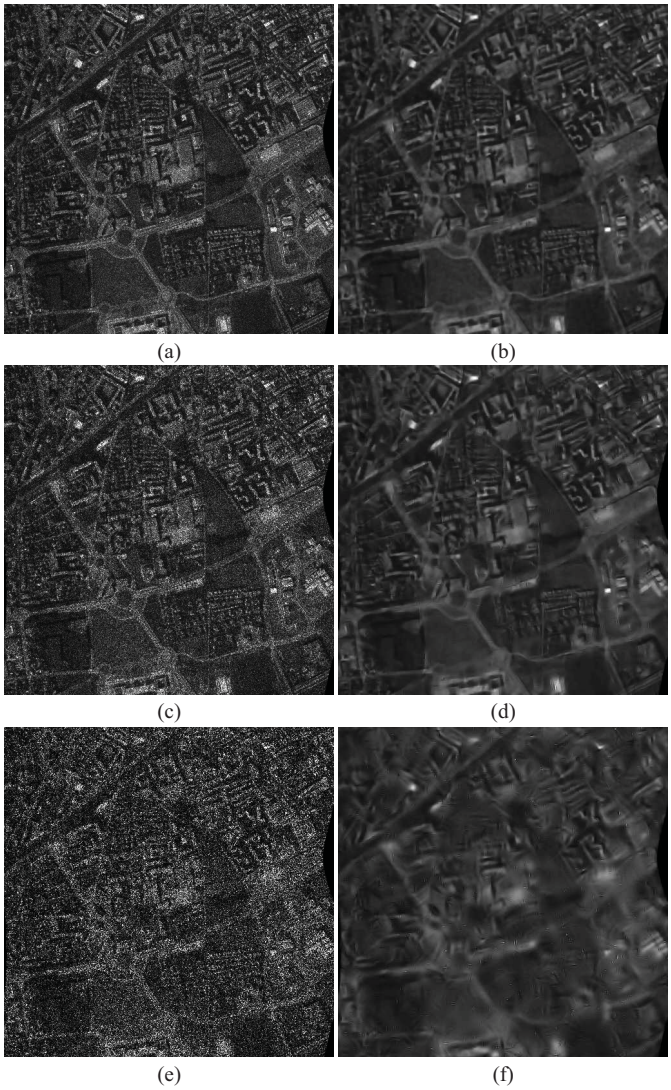

Fig. 7. Experiment with the *Nimes* image. (a) Noisy image, $L = 10$, $RE = 0.315$. (b) Restored image using our method, $RE = 0.163$. (c) Noisy image, $L = 4$, $RE = 0.501$. (d) Restored image using our method, $RE = 0.207$. (e) Noisy image, $L = 1$, $RE = 1.001$. (f) Restored image using our method, $RE = 0.290$.

E. Results on Real SAR Data

In the second set of experiments, we use the real SAR images shown in Fig. 10(a) and (b). These images were collected using the Sandia National Laboratories Twin Otter SAR sensor payload operating at X band. Since the true reflectivity fields are not available, we use ENL to measure the performance of our method. The value of ENL is estimated from the two 32×32 homogeneous regions (shown with white boxes). We refer to the region left side of the image as R1 and the right side of the image as R2. The estimated ENL values are reported in Table II. As can be seen from this table, our method outperforms the WT, MCA, and SBT methods.

TABLE I
RES FOR VARIOUS EXPERIMENTS

Image	L	Noisy	Ours	SBT [40]	MIDAL [21]	[25]	[22]	WT	Lee	MCA
Cameraman	13	0.277	**0.083**	0.104	0.090	-	0.098	0.098	0.170	0.090
Cameraman	10	0.315	**0.090**	0.111	0.097	0.091	-	0.105	0.171	0.101
Cameraman	4	0.498	**0.118**	0.144	0.124	0.131	-	0.135	0.178	0.140
Cameraman	3	0.573	**0.129**	0.156	0.130	-	0.151	0.147	0.182	0.151
Cameraman	1	0.990	0.184	0.220	**0.167**	0.192	-	0.228	0.211	0.210
Fields	10	0.316	**0.054**	0.058	0.056	0.055	-	0.063	0.063	0.052
Fields	4	0.500	**0.065**	0.073	0.066	0.066	-	0.077	0.804	0.071
Fields	1	1.000	0.099	0.114	**0.089**	0.096	-	0.159	0.135	0.110
Nimes	10	0.315	**0.163**	0.312	0.170	0.174	-	0.195	0.273	0.186
Nimes	4	0.501	**0.207**	0.223	0.217	0.217	-	0.247	0.277	0.221
Nimes	1	1.001	**0.290**	0.312	0.301	0.314	-	0.346	0.298	0.320

TABLE II
ESTIMATED ENL VALUES

Image	Region	Original	WT	SBT	Ours	Lee	MCA
Fig. 11(a)	R1	3.291	30.366	49.028	**79.357**	5.518	50.23
Fig. 11(a)	R2	3.236	30.428	84.936	**133.962**	8.263	90.89
Fig. 12(b)	R1	4.117	44.717	75.041	**146.379**	11.35	85.75
Fig. 12(b)	R2	3.997	37.253	74.641	**101.491**	11.30	86.70

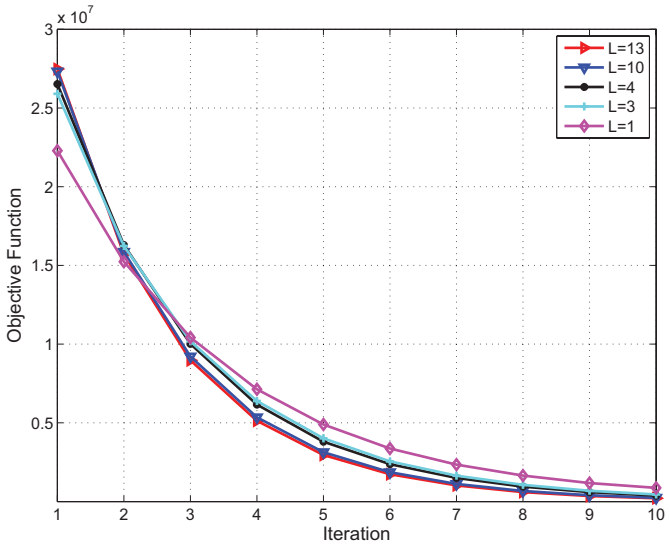

Fig. 8. Objective function value as a function of the iteration number for the experiments with a *Cameraman* image with various numbers of looks.

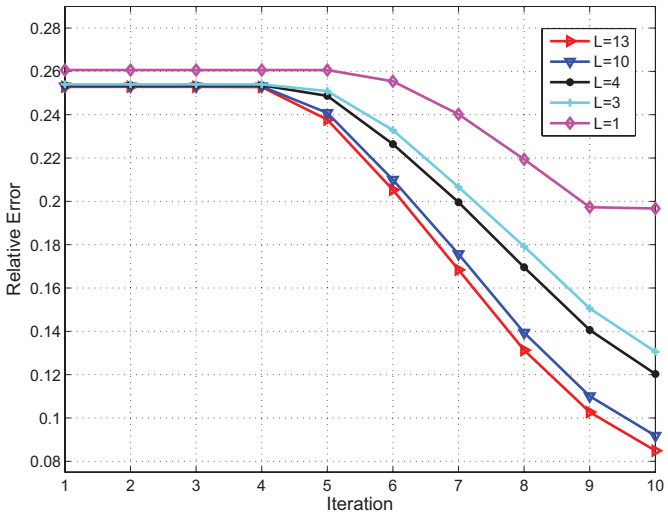

Fig. 9. RE versus number of iteration curves for the experiments with a *Cameraman* image with various numbers of looks.

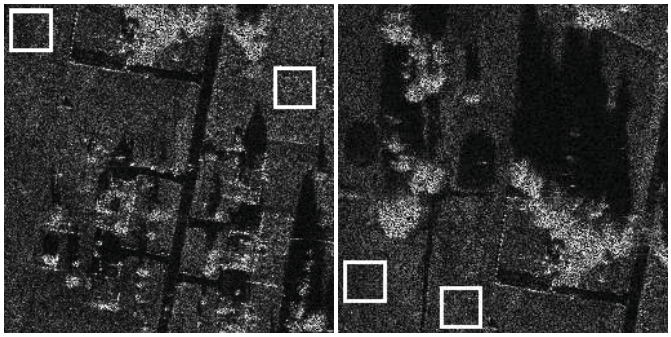

Fig. 10. Real SAR images used for the experiments.

The despeckling results from various methods are shown in Figs. 11(b)–(d) and 12(b)–(d). The ratios of the original image to the filtered images, referred to as the noise images, are shown in Figs. 11(e)–(h) and 12(e)–(h). It is evident from these figures the single dictionary-based reconstructions such as SBT and WT suffer from noticeable artifacts. The MCA method based on curvelets and 2D-DCT provides good reconstruction, but it removes a lot of point targets. Our combined dictionary approach clearly provides good reconstructions and removes most, if not all, of these artifacts and preserves point targets. Note that we have not compared our method on the real SAR images with the other methods since their implementations were not available to us.

F. Computational Efficiency

In our image separation-based despeckling method, the most computationally intensive part is in finding the coefficients from a shearlet dictionary. Using MATLAB on a Windows system with an Intel Core 2 CPU 2.16 GHz/3.00 GB processor, one iteration of the entire algorithm takes around 4.15 s. On average, our method takes about 45 s to process an image

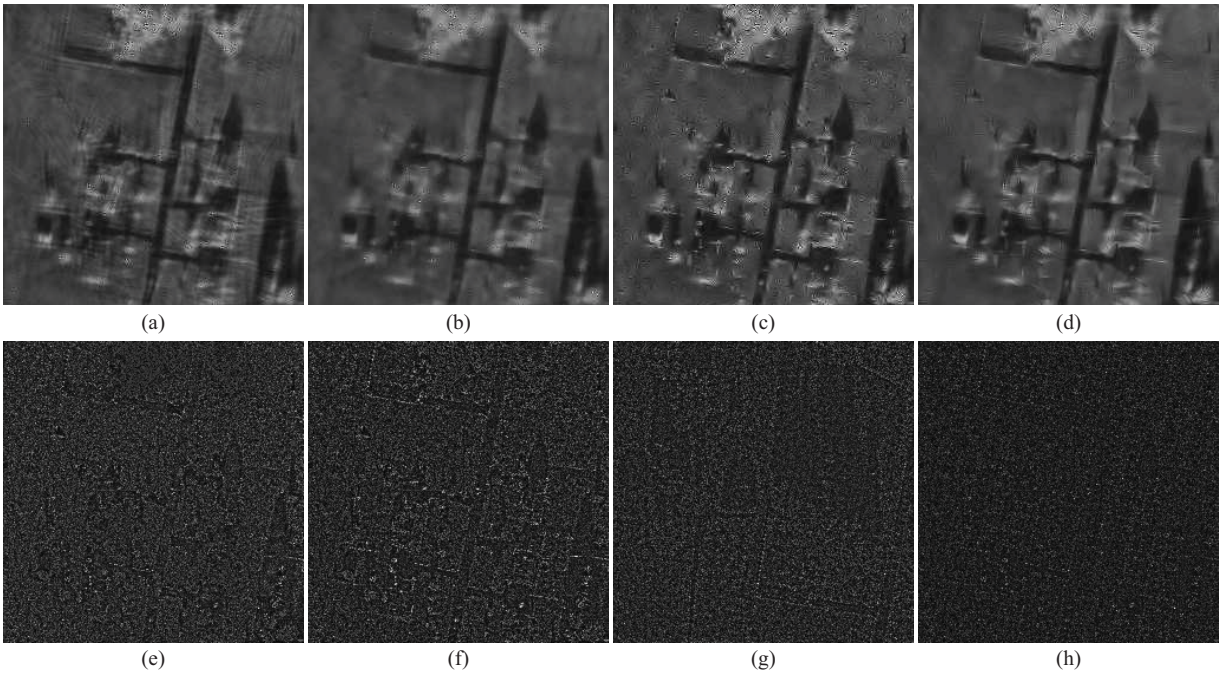

Fig. 11. Despeckled images. Restored using (a) SBT method, (b) MCA method, (c) WT, and (d) our method. (e)–(h) are the noise images corresponding to the filtered images in (a)–(d), respectively.

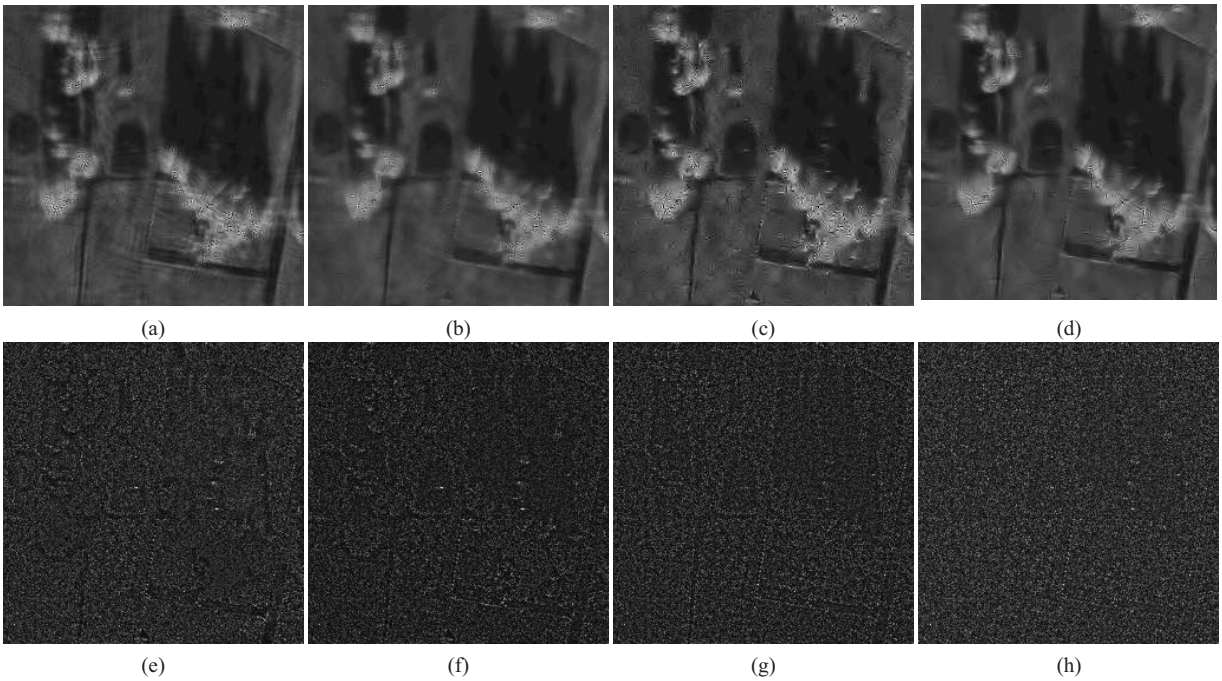

Fig. 12. Despeckled images. Restored using (a) SBT method, (b) MCA method, (c) WT and (d) our method. (e)–(h) are the noise images corresponding to the filtered images in (a)–(d), respectively.

of size 256×256. The performance of our algorithm can be enhanced by using a more efficient shearlet transform implementation which is parallelizable. Each iteration of our algorithm has the complexity of $\mathcal{O}(N^2 \log_2(N))$.

G. Discussion

Note that we have applied our component separation method on the log-transformed images. However, one can directly apply this method on the SAR image without applying the log transformation to separate the piecewise smooth component and the texture component. For instance, SAR model (1) can be rewritten as

$$\begin{aligned} \mathbf{y} &= \mathbf{xf} \\ &= \mathbf{x} + (\mathbf{f} - \mathbf{1})\mathbf{x} \end{aligned} \tag{27}$$

where $\mathbf{1} = [1, \ldots, 1]^T$. In this setting, the first and the second term in (27) can be viewed as $\mathbf{x}_p$ and $\mathbf{x}_t$, respectively. In particular, if one has designed dictionaries specifically to compress

these terms, then one can view the first term as the restored image. However, designing dictionaries to compress the individual terms in (27) is nontrivial. One can adapt dictionary learning methods [44] to learn these components. This in turn would require a collection of training images containing only the piecewise smooth reflectivity fields and images containing only signal-dependent noise. This formulation is also relevant in the case when SAR images contain a strong additive noise component where the purely multiplicative model may not be adequate.

V. Conclusion

We proposed a new method of speckle reduction in SAR imagery based on separating an image into various components. Unique to this approach is the ability to use specific dictionaries of representations suited for separation with an iterative scheme that is able to retain important features. Experiments showed that this method performs favorably compared to other competitive methods. This new process is also valuable for many SAR image understanding tasks such as road detection, railway detection, ship wake detection, texture segmentation for agricultural scenes, and coastline detection. In addition, specific dictionaries could be designed to be used with this procedure to capture unique signatures while dealing with speckle removal.

Appendix
Shearlet Transform

The shearlet construction can be considered a natural extension of wavelets into two dimensions [45]. Its representative elements are defined by the 2-D affine system

$$\{\tilde{\psi}_{\text{ast}}(x) = |\det M_{as}|^{-\frac{1}{2}}\, \tilde{\psi}(M_{as}^{-1}x - t) :\ t \in \mathbb{R}^2\}$$

where

$$M_{as} = \begin{pmatrix} 1 & s \\ 0 & 1 \end{pmatrix} \begin{pmatrix} a & 0 \\ 0 & \sqrt{a} \end{pmatrix} \tag{28}$$

is a product of a shearing and anisotropic dilation matrix for $(a, s) \in R^+ \times R$. The generating function $\tilde{\psi}$ is such that

$$\tilde{\Psi}(\xi) = \tilde{\Psi}(\xi_1, \xi_2) = \tilde{\Psi}_1(\xi_1)\tilde{\Psi}_2\left(\frac{\xi_2}{\xi_1}\right)$$

where $\tilde{\psi_1}$ is a continuous wavelet for which $\tilde{\Psi}_1 \in C^\infty(R)$ with $\operatorname{supp}\tilde{\Psi}_1 \subset [-2, 1/2] \cup [1/2, 2]$, and $\tilde{\psi_2}$ is chosen so that $\tilde{\Psi}_2 \in C^\infty(\mathbb{R})$, $\operatorname{supp}\tilde{\Psi}_2 \subset [-1, 1]$, with $\tilde{\Psi}_2 > 0$ on $(-1, 1)$, and $\|\tilde{\psi_2}\|_2 = 1$. Under these assumptions, a function $f \in L^2(\mathbb{R}^2)$ can be represented as

$$f(x) = \int_{\mathbb{R}^2} \int_{-\infty}^{\infty} \int_0^{\infty} \langle f, \tilde{\psi}_{\text{ast}} \rangle\, \tilde{\psi}_{\text{ast}}(x) \frac{da}{a^3}\, ds\, dt$$

for $a \in \mathbb{R}^+$, $s \in \mathbb{R}$, and $t \in \mathbb{R}^2$. The operator $\mathcal{SH}$ defined by

$$\mathcal{SH}f(a, s, t) = \langle f, \tilde{\psi}_{\text{ast}} \rangle$$

is referred to as the continuous shearlet transform of $f \in L^2(\mathbb{R})$. It is dependent on the scale variable a, the shear s, and the location t.

The collection of discrete shearlets is given by

$$\{\tilde{\psi}_{j,\ell,k} = |\det A|^{j/2}\, \tilde{\psi}(B^\ell A^j x - k) :\ j, \ell \in \mathbb{Z}, k \in \mathbb{Z}^2\} \tag{29}$$

where

$$B = \begin{pmatrix} 1 & 1 \\ 0 & 1 \end{pmatrix} \qquad A = \begin{pmatrix} 2 & 0 \\ 0 & \sqrt{2} \end{pmatrix}. \tag{30}$$

Shearlets form a Parseval frame (tight frame with bounds equal to 1) for $L^2(\mathbb{R}^2)$, given the appropriate choice of the generating function $\tilde{\psi}$ (see [41] for details). An M-channel filterbank implementation can be done by using the techniques given in [46]. As a consequence, its implementation has a complexity of $\mathcal{O}(N^2 \log_2(N))$ for an $N \times N$ image.

References

[1] J. W. Goodman, "Some fundamental properties of speckle," *J. Opt. Soc. Amer.*, vol. 66, no. 11, pp. 1145–1150, Nov. 1976.

[2] C. Oliver and S. Quegan, *Understanding Synthetic Aperture Radar Images*. Norwood, MA, USA: Artech House, 1998.

[3] M. Amirmazlaghani and H. Amindavar, "Two novel Bayesian multiscale approaches for speckle suppression in SAR images," *IEEE Trans. Geosci. Remote Sens.*, vol. 48, no. 7, pp. 2980–2993, Jul. 2010.

[4] G. Moser and S. B. Serpico, "Generalized minimum-error thresholding for unsupervised change detection from SAR amplitude imagery," *IEEE Trans. Geosci. Remote Sens.*, vol. 44, no. 10, pp. 2972–2982, Oct. 2006.

[5] F. Argenti, T. Bianchi, A. Lapini, and L. Alparone, "Fast MAP despeckling based on Laplacian-Gaussian modeling of wavelet coefficients," *IEEE Geosci. Remote Sens. Lett.*, vol. 9, no. 1, pp. 13–17, Jan. 2012.

[6] D. Gleich and M. Datcu, "Wavelet-based despeckling of SAR images using Gauss–Markov random fields," *IEEE Trans. Geosci. Remote Sens.*, vol. 45, no. 12, pp. 4127–4143, Dec. 2007.

[7] H.-C. Li, W. Hong, Y.-R. Wu, and P.-Z. Fan, "An efficient and flexible statistical model based on generalized gamma distribution for amplitude SAR images," *IEEE Trans. Geosci. Remote Sens.*, vol. 48, no. 6, pp. 2711–2722, Jun. 2010.

[8] J.-S. Lee, "Digital image enhancement and noise filtering by use of local statistics," *IEEE Trans. Pattern Anal. Mach. Intell.*, vol. PAMI-2, no. 2, pp. 165–168, Mar. 1980.

[9] D. T. Kuan, A. A. Sawchuk, T. C. Strand, and P. Chavel, "Adaptive noise smoothing filter for images with signal-dependent noise," *IEEE Trans. Pattern Anal. Mach. Intell.*, vol. PAMI-7, no. 2, pp. 165–177, Mar. 1985.

[10] R. Touzi, "A review of speckle filtering in the context of estimation theory," *IEEE Trans. Geosci. Remote Sens.*, vol. 40, no. 11, pp. 2392–2404, Nov. 2002.

[11] M. Walessa and M. Datcu, "Model-based despeckling and information extraction from SAR images," *IEEE Trans. Geosci. Remote Sens.*, vol. 38, no. 5, pp. 2258–2269, Sep. 2000.

[12] H. Xie, L. E. Pierce, and F. T. Ulaby, "SAR speckle reduction using wavelet denoising and Markov random field modeling," *IEEE Trans. Geosci. Remote Sens.*, vol. 40, no. 10, pp. 2196–2212, Oct. 2002.

[13] F. Argenti and L. Alparone, "Speckle removal from SAR images in the undecimated wavelet domain," *IEEE Trans. Geosci. Remote Sens.*, vol. 40, no. 11, pp. 2363–2374, Nov. 2002.

[14] A. Achim, P. Tsakalides, and A. Bezerianos, "SAR image denoising via Bayesian wavelet shrinkage based on heavy-tailed modeling," *IEEE Trans. Geosci. Remote Sens.*, vol. 41, no. 8, pp. 1773–1784, Aug. 2003.

[15] M. Dai, C. Peng, A. K. Chan, and D. Loguinov, "Bayesian wavelet shrinkage with edge detection for SAR image despeckling," *IEEE Trans. Geosci. Remote Sens.*, vol. 42, no. 8, pp. 1642–1648, Aug. 2004.

[16] S. Foucher, G. B. Benie, and J.-M. Boucher, "Multiscale MAP filtering of SAR images," *IEEE Trans. Geosci. Remote Sens.*, vol. 10, no. 1, pp. 49–60, Jan. 2001.

[17] H. Guo, J. E. Odegard, M. Lang, R. A. Gopinath, I. W. Selesnick, and C. S. Burrus, "Wavelet based speckle reduction with application to SAR ATD/R," in *Proc. Int. Conf. Image Process.*, vol. 1. Nov. 1994, pp. 75–79.

[18] D. L. Donoho, "De-noising by soft-thresholding," *IEEE Trans. Inf. Theory*, vol. 41, no. 3, pp. 613–627, May 1995.

[19] D. L. Donoho and J. M. Johnstone, "Ideal spatial adaptation by wavelet shrinkage," *Biometrika*, vol. 81, no. 3, pp. 425–455, 1994.

[20] L. I. Rudin, S. Osher, and E. Fatemi, "Nonlinear total variation based noise removal algorithms," *Phys. D*, vol. 60, nos. 1–4, pp. 259–268, Nov. 1992.

[21] J. M. Bioucas-Dias and M. A. T. Figueiredo, "Multiplicative noise removal using variable splitting and constrained optimization," *IEEE Trans. Image Process.*, vol. 19, no. 7, pp. 1720–1730, Jul. 2010.

[22] Y.-M. Huang, M. K. Ng, and Y.-W. Wen, "A new total variation method for multiplicative noise removal," *SIAM J. Img. Sci.*, vol. 2, no. 1, pp. 20–40, Jan. 2009.

[23] G. Aubert and J.-F. Aujol, "A variational approach to remove multiplicative noise," *SIAM J. Appl. Math.*, vol. 68, no. 4, pp. 925–946, Jan. 2008.

[24] M. Nikolova, "Weakly constrained minimization: Application to the estimation of images and signals involving constant regions," *J. Math. Imag. Vis.*, vol. 21, no. 2, pp. 155–175, Sep. 2004.

[25] S. Durand, J. Fadili, and M. Nikolova, "Multiplicative noise removal using L1 fidelity on frame coefficients," *J. Math. Imag. Vis.*, vol. 36, no. 3, pp. 201–226, Mar. 2010.

[26] R. R. Coifman and D. L. Donoho, *Translation-Invariant De-Noising*, A. Antoniadis and G. Oppenheim, Eds. New York, USA: Springer-Verlag, 1995.

[27] M. J. Fadili, J.-L. Starck, and L. Boubchir, "Morphological diversity and sparse image denoising," in *Proc. IEEE Int. Conf. Acoust. Speech Signal Process.*, vol. 1. Apr. 2007, pp. 589–592.

[28] J. Starck, E. J. Candes, and D. L. Donoho, "Very high quality image restoration by combining wavelets and curvelets," *Proc. SPIE*, vol. 4478, pp. 9–19, Dec. 2001.

[29] J.-F. Aujol, G. Aubert, L. Blanc-Féraud, and A. Chambolle, "Image decomposition application to SAR images," in *Proc. 4th Int. Conf. Scale Space Methods Comput. Vis.*, 2003, pp. 297–312.

[30] J.-L. Starck, M. Elad, and D. L. Donoho, "Image decomposition via the combination of sparse representations and a variational approach," *IEEE Trans. Image Process.*, vol. 14, no. 10, pp. 1570–1582, Oct. 2005.

[31] F. Ulaby and M. C. Dobson, *Handbook of Radar Scattering Statistics for Terrain*. Norwood, MA, USA: Artech House, 1989.

[32] H. Xie, L. Pierce, and F. Ulaby, "Statistical properties of logarithmically transformed speckle," *IEEE Trans. Geosci. Remote Sens.*, vol. 40, no. 3, pp. 721–727, Mar. 2002.

[33] C. Tison, J.-M. Nicolas, F. Tupin, and H. Maitre, "A new statistical model for Markovian classification of urban areas in high-resolution SAR images," *IEEE Trans. Geosci. Remote Sens.*, vol. 42, no. 10, pp. 2046–2057, Oct. 2004.

[34] S. Sardy, A. G. Bruce, and P. Tseng, "Block coordinate relaxation methods for nonparametric wavelet denoising," *J. Comput. Graph. Stat.*, vol. 9, no. 2, pp. 361–379, 2000.

[35] M. Elad, *Sparse and Redundant Representations: From Theory to Applications in Signal and Image Processing*. New York, USA: Springer-Verlag, 2010.

[36] I. Daubechies, M. Defrise, and C. De Mol, "An iterative thresholding algorithm for linear inverse problems with a sparsity constraint," *Commun. Pure Appl. Math.*, vol. 57, no. 11, pp. 1413–1541, Nov. 2004.

[37] M. Zibulevsky and M. Elad, "L1-L2 optimization in signal and image processing," *IEEE Signal Process. Mag.*, vol. 27, no. 3, pp. 76–88, May 2010.

[38] J.-L. Starck, F. Murtagh, and J. M. Fadili, *Sparse Image and Signal Processing: Wavelets, Curvelets, Morphological Diversity*. Cambridge, U.K.: Cambridge Univ. Press, 2010.

[39] G. Steidl, J. Weickert, T. Brox, P. Mrázek, and M. Welk, "On the equivalence of soft wavelet shrinkage, total variation diffusion, total variation regularization, and SIDEs," *SIAM J. Numer. Anal.*, vol. 42, no. 2, pp. 686–713, May 2004.

[40] C. Chesneaua, J. Fadili, and J.-L. Starck, "Stein block thresholding for image denoising," *Appl. Comput. Harmon. Anal.*, vol. 28, no. 1, pp. 67–88, Jan. 2010.

[41] G. R. Easley, D. Labate, and W. Q. Lim, "Sparse directional image representations using the discrete shearlet transform," *Appl. Comput. Harmon. Anal.*, vol. 25, no. 1, pp. 25–46, Jul. 2008.

[42] V. M. Patel, G. R. Easley, and D. M. Healy, "Shearlet-based deconvolution," *IEEE Trans. Image Process.*, vol. 18, no. 12, pp. 2673–2685, Dec. 2009.

[43] J. Bobin, J.-L. Starck, J. Fadili, Y. Moudden, and D. L. Donoho, "Morphological component analysis: An adaptive thresholding strategy," *IEEE Trans. Image Process.*, vol. 16, no. 11, pp. 2675–2681, Nov. 2007.

[44] M. Aharon, M. Elad, and A. M. Bruckstein, "The K-SVD: An algorithm for designing of overcomplete dictionaries for sparse representation," *IEEE Trans. Signal Process.*, vol. 54, no. 11, pp. 4311–4322, Nov. 2006.

[45] D. Labate, G. K. W.-Q. Lim, and G. Weiss, "Sparse multidimensional representation using shearlets," *Proc. SPIE*, vol. 5914, pp. 254–262, Jul. 2005.

[46] G. R. Easley, V. M. Patel, and J. D. M. Healy, "An M-channel directional filter bank compatible with the contourlet and shearlet frequency tiling," *Proc. SPIE*, vol. 6701, pp. 1–11, Sep. 2007.

Vishal M. Patel (M'01) received the B.S. degrees in electrical engineering and applied mathematics (Hons.) and the M.S. degree in applied mathematics from North Carolina State University, Raleigh, NC, USA, in 2004 and 2005, respectively, and the Ph.D. degree in electrical engineering from the University of Maryland, College Park, MD, USA, in 2010. He received an ORAU Post-Doctoral Fellowship in 2010.

He is a member of the Research Faculty with the University of Maryland Institute for Advanced Computer Studies (UMIACS). His current research interests include signal processing, computer vision and pattern recognition with applications to biometrics and imaging.

Dr. Patel is a member of Eta Kappa Nu, Pi Mu Epsilon, and Phi Beta Kappa.

Glenn R. Easley (M'08) received the B.S. (Hons.) and M.A. degrees in mathematics from the University of Maryland, College Park, MD, USA, in 1993 and 1996, respectively, and the Ph.D. degree in computational science and informatics from George Mason University, Fairfax VA, USA, in 2000.

He has been with System Planning Corporation since 2000, working on signal, image and computer vision problems. He has also been a Visiting Assistant Professor with the Norbert Wiener Center, University of Maryland, from 2005 to 2009. His current research interests include computational harmonic analysis, with special emphasis on wavelet theory and time-frequency analysis, synthetic aperture radar, inverse problems, and computer vision.

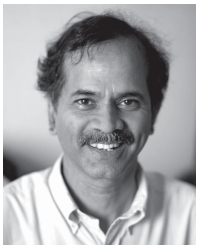

Rama Chellappa (F'92) received the B.E. (Hons.) degree in electronics and communication engineering from the University of Madras, Chennai, India, in 1975, the M.E. (with Distinction) degree from the Indian Institute of Science, Bangalore, India, in 1977, and the M.S.E.E. and Ph.D. degrees in electrical engineering from Purdue University, West Lafayette, IN, USA, in 1978 and 1981, respectively.

He was a Faculty Member with the Department of Electrical Engineering/Systems, University of Southern California (USC), from 1981 to 1991. Since 1991, he has been a Professor of electrical and computer engineering (ECE) and an affiliate Professor of computer science with the University of Maryland (UMD), College Park, MD, USA. He is also affiliated with the Center for Automation Research and the Institute for Advanced Computer Studies (Permanent Member) and is serving as the Chair of the ECE Department. In 2005, he was named a Minta Martin Professor of Engineering. He holds three patents. His current research interests include face recognition, clustering and video summarization, 3D modeling from video, image and video-based recognition of objects, events and activities, dictionary-based inference, compressive sensing, domain adaptation and hyper spectral processing.

Dr. Chellappa was the recipient of an NSF Presidential Young Investigator Award, four IBM Faculty Development Awards, an Excellence in Teaching Award from the School of Engineering at USC, and two paper awards from the International Association of Pattern Recognition (IAPR). He is a recipient of the K.S. Fu Prize from IAPR. He received the Society, Technical Achievement and Meritorious Service Awards from the IEEE Signal Processing Society. He was also the recipient of the Technical Achievement and Meritorious Service Awards from the IEEE Computer Society. At UMD, he was elected as a Distinguished Faculty Research Fellow and Distinguished Scholar-Teacher, received an Outstanding Innovator Award from the Office of Technology Commercialization, and received an Outstanding GEMSTONE Mentor Award from the Honors College. He received the Outstanding Faculty Research Award and the Poole and Kent Teaching Award for Senior Faculty from the College of Engineering. In 2010, he was recognized as an Outstanding ECE by Purdue University. He is a Fellow of IAPR, OSA and AAAS.

Prof. Chellappa served as the Editor-in-Chief of the IEEE transactions on Pattern Analysis and Machine Intelligence. He has served as a General and Technical Program Chair for several IEEE international and national conferences and workshops. He is a Golden Core Member of the IEEE Computer Society and served as a Distinguished Lecturer of the IEEE Signal Processing Society. Recently, he completed a two-year term as the President of the IEEE Biometrics Council.

Nasser M. Nasrabadi (S'80–M'84–SM'92–F'01) received the B.Sc. (Eng.) and Ph.D. degrees in electrical engineering from the Imperial College of Science and Technology (University of London), London, U.K., in 1980 and 1984, respectively.

He worked for IBM, London, U.K., as a Senior Programmer from October 1984 to December 1984. From 1985 to 1986, he was with Philips Research Laboratory, New York, NY, USA, as a Technical Staff Member. From 1986 to 1991, he was an Assistant Professor with the Department of Electrical Engineering, Worcester Polytechnic Institute, Worcester, MA, USA. From 1991 to 1996, he was an Associate Professor with the Department of Electrical and Computer Engineering, State University of New York at Buffalo, Buffalo, NY. Since September 1996, he has been a Senior Research Scientist (ST) with the U.S. Army Research Laboratory (ARL) working on image processing and automatic target recognition. His current research interests include hyperspectral imaging, automatic target recognition, statistical machine learning theory, robotics, and neural networks applications to image processing.

Dr. Nasrabadi has served as an Associate Editor for the IEEE TRANSACTIONS ON IMAGE PROCESSING, the IEEE TRANSACTIONS ON CIRCUITS, SYSTEMS AND VIDEO TECHNOLOGY, and the IEEE TRANSACTIONS ON NEURAL NETWORKS. He is a Fellow of ARL and SPIE.